Evolution of Denmark Strait Overflow Cyclones and Their Relationship to Overflow Surges

M. Almansi[1]*, T. W. N. Haine[1], R. Gelderloos[1], and R. S. Pickart[2]

[1]Department of Earth and Planetary Sciences, The Johns Hopkins University

[2]Woods Hole Oceanographic Institution

Key Points:

- High-transport events associated with the Denmark Strait Overflow (DSO) evolve into DSO cyclones downstream.
- The underlying dynamics of the DSO cyclones differ between two different types of high-transport events.
- The potential vorticity of DSO cyclones is only materially conserved during their growth phase.

*301 Olin Hall - 3400 N. Charles Street, Baltimore, MD 21218, USA

Corresponding author: Mattia Almansi, mattia.almansi@jhu.edu

Abstract

Mesoscale features present at the Denmark Strait sill regularly enhance the volume transport of the Denmark Strait Overflow (DSO). They are important for the Atlantic Meridional Overturning Circulation, and ultimately, for the global climate system. Using a realistic numerical model, we find new evidence of the causal relationship between high-transport events and DSO cyclones observed downstream. Most of the cyclones form at the Denmark Strait sill during overflow surges and, because of potential vorticity conservation and stretching of the water column, grow as they move equatorward. A fraction of the cyclones form downstream of the sill, when anticyclonic vortices formed during high-transport events start collapsing. Regardless of their formation mechanism, DSO cyclones weaken starting roughly 150 km downstream of the sill, and potential vorticity is only materially conserved during the growth phase.

Plain Language Summary

Ocean currents affecting the global climate are sustained by cold and dense water that sinks in the North Atlantic Ocean. A large portion of this water passes through the Denmark Strait, which is a channel between Greenland and Iceland. The amount of water entering the strait varies from day to day, and is controlled by ocean vortices. Knowing the mechanisms associated with these vortices is of key importance for understanding and predicting the Earths climate. Using a realistic numerical model, we find that the vortices are generated in the strait during dense water surges. In one scenario, the ocean vortices cross Denmark Strait rotating in the same direction as the Earth (counterclockwise). These vortices strengthen as they move towards the south. If the vortices initially rotate clockwise, they move slowly and quickly collapse. The water converging south of them triggers the formation of new vortices rotating counterclockwise. All of these energetic vortices move towards the equator. First they quickly grow, then they lose energy starting roughly 150 kilometers south of Denmark Strait.

1 Introduction

The Denmark Strait is an ocean channel located between Greenland and Iceland (Figure 1a). It is a gateway between the Nordic Seas and the subpolar North Atlantic. The Denmark Strait Overflow (DSO) is a bottom-trapped current transporting dense water equatorward. After crossing Denmark Strait, the DSO volume flux (transport) in-

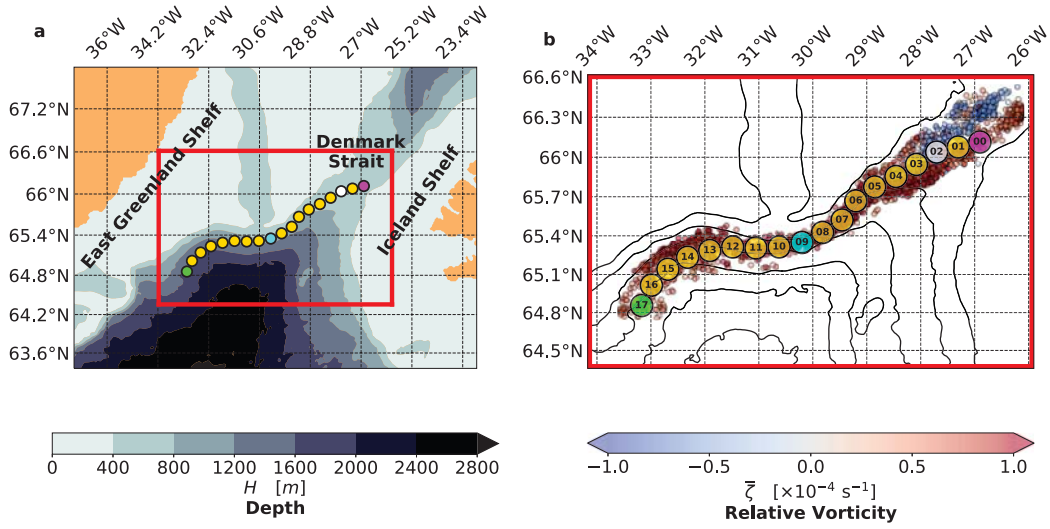

Figure 1. (a) Seafloor bathymetry in the region of interest for this study. Red lines bound the area fed to the vortex detection algorithm. (b) Location of the centers of the detected vortices color-coded by their mean relative vorticity ($\bar{\zeta}$) at a depth of $5H/8$. Black contours show the bathymetry (same interval used in a). Circles indicate the stations along the DSO path. Circles colored in magenta, white, blue, and green indicate where the DSO path crosses hydrographic sections known as the Látrabjarg Line (LL), Denmark Strait South (DSS), Transient Tracers in the Ocean (TTO), and Spill Jet (SJ), respectively.

creases rapidly by entrainment (Dickson & Brown, 1994) and supports the Atlantic Meridional Overturning Circulation (AMOC). The East Greenland Current system (EGC), which involves two separate branches (Våge et al., 2013), flows southward along the East Greenland coast and contributes about two thirds of the DSO transport at the sill (Harden et al., 2016). The remaining third of DSO water is transported primarily by the North Icelandic Jet (NIJ; Jonsson & Valdimarsson, 2004; Semper et al., 2019), which flows towards Denmark Strait along the north side of Iceland. The poleward flowing North Icelandic Irminger Current (NIIC) is another contributor to the DSO water.

Studies on the DSO transport have found no long-term trends (Jochumsen et al., 2012, 2017). Both observations and numerical models show a pronounced high-frequency variability (from one day to one week at the sill; Ross, 1984; Macrander et al., 2007; Haine, 2010; von Appen et al., 2017). Cooper (1955) characterized thick lenses of overflow water associated with high volume fluxes known as "boluses", and Mastropole et al. (2017) found boluses in about 40% of a 20-year collection of shipboard measurements. "Pulses"

are another dominant mesoscale feature occurring every five days at the Denmark Strait sill. They are associated with a thinning and acceleration of the DSO layer (von Appen et al., 2017). Boluses and pulses augment the yearly mean transport of the DSO by about 30% (Almansi et al., 2017). Moritz et al. (2019) found that high-transport events at the sill occasionally correspond to anticyclonic eddies. Spall et al. (2019) characterized a third type of mesoscale feature referred to as "flooding events". During these events, the NIIC migrates westward, and the deepest part of the sill is filled with subtropical-origin water. Boluses, pulses, and flooding events are all associated with the meandering of the hydrographic front in Denmark Strait (Spall et al., 2019).

Downstream of Denmark Strait, the high-frequency variability of the overflow is dominated by the presence of energetic features known as "DSO cyclones". The first studies of these features used laboratory experiments (Whitehead et al., 1990), satellite imagery (Bruce, 1995), and surface drifter trajectories to describe their basic characteristics (Krauss, 1996). Several studies then explored the underlying dynamics of the cyclones (Krauss & Käse, 1998; Spall & Price, 1998; Jungclaus et al., 2001; Shi et al., 2001; Reszka et al., 2002). Spall and Price (1998) formulated the so called "PV Outflow Hypothesis". Cyclogenesis in their three-layer model was explained via conservation of potential vorticity (PV) in the presence of strong vortex stretching. von Appen et al. (2014) found that DSO cyclones represent the largest source of variability roughly 300 km downstream of Denmark Strait. Although the model results of Spall and Price (1998) indicate that these features can form from a steady overflow, von Appen et al. (2017) hypothesized a one-to-one connection between the passage of boluses/pulses and the formation of DSO cyclones.

Characterizing the DSO high-frequency fluctuations is of key importance for understanding and predicting the AMOC variability. At present, the notion of a causal relationship between the mesoscale variability at the sill and the downstream cyclones remains a hypothesis which needs to be investigated further. In this paper, we present new evidence for the existence of this relationship. We also investigate how different types of high-transport events trigger the formation of DSO cyclones, and describe their evolution along the DSO path.

2 Materials and Methods

2.1 Numerical circulation model

We fill the gaps in the sparse measurements along the DSO path using a yearlong, high-resolution, realistic circulation model. The dynamics are simulated using the Massachusetts Institute of Technology General Circulation Model (MITgcm; Marshall et al., 1997). An identical configuration with different atmospheric forcing is described in detail in Almansi et al. (2017). The numerical solutions are publicly available on SciServer (Medvedev et al., 2016), and the additional fields shown in this paper can be reproduced using OceanSpy v0.1 (Almansi et al., 2019). The model is particularly well suited to study mesoscale features occurring on short timescales (1-10 days; Almansi et al., 2017; Spall et al., 2019). Haine et al. (2009) found that the spatial resolution of the atmospheric fields used to force high-resolution models significantly affects the ocean circulation in Denmark Strait. Therefore, we use the 15-km resolution Arctic System Reanalysis (ASRv2; Bromwich et al., 2018), which represents a significant improvement (Bromwich et al., 2016) in horizontal resolution of the atmospheric forcing previously implemented (ERA-Interim; Dee et al., 2011). The model solutions have been also compared to data collected upstream of Denmark Strait by Håvik et al. (2019). Vertical sections of hydrographic and velocity fields are consistent with the validation performed by Almansi et al. (2017). Overall, the agreement between the model and the available observations around Denmark Strait is excellent.

2.2 Detection of mesoscale features

High-transport events and DSO cyclones have been detected independently. Boluses and pulses have been identified using the same criteria as Almansi et al. (2017), whereas DSO cyclones have been detected using an automatic vortex detection scheme based on the Okubo-Weiss parameter (OW; Okubo, 1970; Weiss, 1991). The algorithm operates on terrain-following levels (σ-levels) located in the bottom half of the water column, and isolates mesoscale features with relative vorticity higher than the strain (see the supporting information for more details). The relative vorticity is defined by $\zeta = \frac{\partial v}{\partial x} - \frac{\partial u}{\partial y}$, where $\mathbf{u} = (u, v, w)$ is the vector velocity field written as a function of Cartesian position $x\hat{\mathbf{x}} + y\hat{\mathbf{y}} + z\hat{\mathbf{z}}$. The results shown and discussed hereafter refer to the σ-level at a depth of $5H/8$, where H is the seafloor depth. Figure 1b shows the location

of the centers of the vortices detected. The cyclones ($\bar{\zeta} > 0$; overline indicates a spatial average in the region occupied by the vortex) are located in proximity to the DSO path and move southward along the continental slope. The anticyclones ($\bar{\zeta} < 0$), which are thought to be related to a fraction of DSO cyclones observed at the Spill Jet section (station #17 in Figure 1b; von Appen et al., 2017), are located on the western side of the Denmark Strait trough.

3 Results

3.1 Relationship between DSO cyclones and overflow surges

Boluses are coupled with the cyclones detected near the Denmark Strait sill, whereas pulses are coupled with the anticyclones. Specifically, more than 70% of the cyclones (anticyclones) near station #00 in Figure 1b occur within 48 hours of a bolus (pulse). Figure 2a shows a cyclone crossing Denmark Strait over the deepest part of the sill. At the same time, a bolus was detected at the Látrabjarg Line. The density difference between the snapshot exhibiting the cyclone and the background state (yearly average) highlights positive density anomalies within the perimeter of the cyclone (Figure 2b). As we are investigating density fields along terrain-following surfaces, higher densities ($\Delta\sigma_\theta > 0$) are the result of the shoaling of the deep isopycnals. These anomalies are consistent with the thickening of the overflow layer characteristic of boluses. The vortex detection algorithm identified the same cyclone shown in Figure 2a at different locations downstream of Denmark Strait. The cyclone follows the DSO path, and the mean vorticity of its core ($\bar{\zeta}$) grows as the feature moves to the southwest. Specifically, $\bar{\zeta}$ is about $0.5{\times}10^{-4}$ s^{-1} near the Látrabjarg Line station, and more than twice that value roughly 100 km downstream. As the height of the water column also increases along the path (i.e., stretching of the water column), positive relative vorticity is added to the mesoscale feature due to vortex stretching. As the cyclone moves downstream, it coincides with a relative maximum in density ($\Delta\sigma_\theta > 0$). Therefore, the DSO cyclone and the bolus propagate in phase, and positive density anomalies enter the Irminger Basin.

Figure 2c shows an anticyclone detected near the Látrabjarg Line during a pulse event (January 30th, 2008). In contrast to the cyclone described above, the anticyclone corresponds to a region with instantaneous density lower than the background state (Figure 2d). The deepening of the isopycnals is consistent with the presence of pulses, which

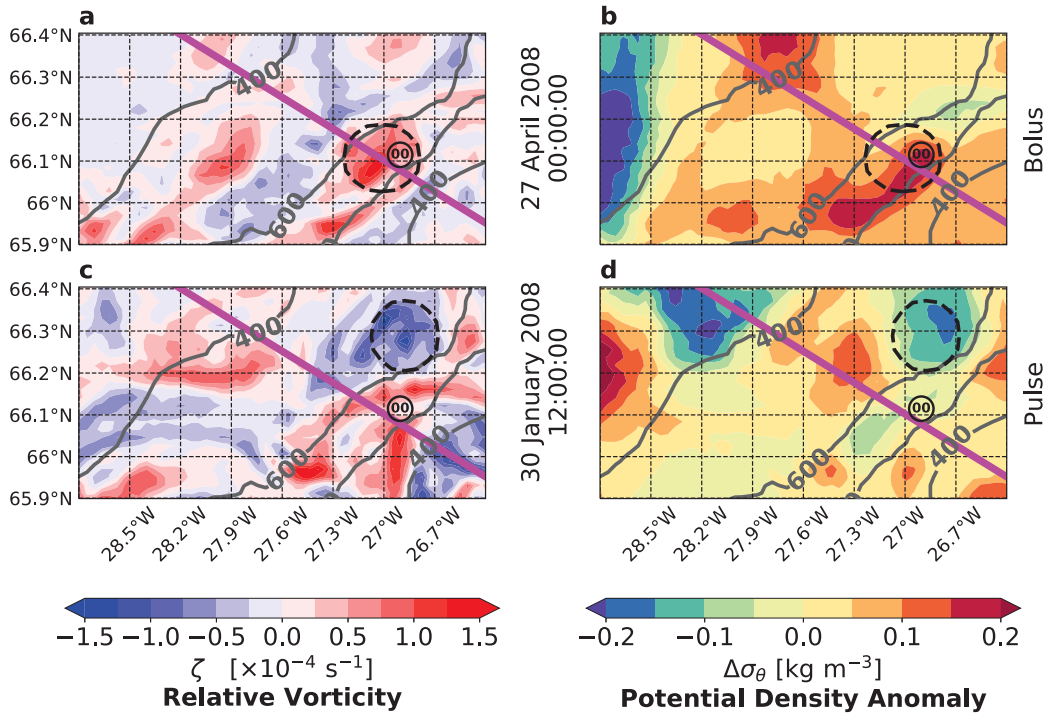

Figure 2. Relative vorticity (a, c) and instantaneous potential density minus the yearly mean (b, d) during a bolus and a pulse. The bolus (a, b) crossed the Látrabjarg Line (drawn in magenta) on April 27th, 2008 at midnight. The pulse (c, d) was detected in Denmark Strait on January 30th, 2008 at noon. Dark gray contours indicate the seafloor depth in meters. Dashed lines bound the vortices detected. The circle #00 indicates the Látrabjarg Line station. The labeling convention of the DSO stations is the same used in Figure 1. Fields have been extracted along the σ-level at a depth of $5H/8$.

enhance the southward volume flux of the overflow and reduce its thickness. The anticyclone in Figure 2c has been identified by the vortex detection algorithm in multiple successive snapshots (Figure 3). It crosses Denmark Strait on the western side of the trough and slowly veers towards Greenland (unlike the cyclones crossing Denmark Strait which propagate quickly to the southwest). This same orientation of the flow was found by Almansi et al. (2017) in the composite of pulse events. The path followed by the anticyclone suggests that the 400-meter isobath prevents the feature from reaching the East Greenland shelf. As the vortex moves toward the shelf, the anticyclonic relative vorticity is sustained by the shrinking of the water column ($\bar{\zeta} \simeq -0.7 \times 10^{-4}$ s^{-1}). When the anticyclone reaches the western side of the trough, bands of positive relative vorticity surround the slowly-moving core of the anticyclone (Figure 3a). At the same time, the absolute magnitude of $\bar{\zeta}$ decreases. As the anticyclone weakens, the peripheral bands of positive relative vorticity strengthen and converge, triggering the formation of a cyclone south of the collapsing anticyclone. The cyclone starts emerging in Figure 3b (near station #05), but its vorticity exceeds the strain between stations #07 and #08 (Figure 3d), where the cyclone is identified by the vortex detector. The cyclonic feature triggered by the anticyclone moves southwestward following the DSO path, and it gains positive relative vorticity due to stretching of the water column as it moves downstream. The geometry and relative vorticity magnitude of the detected cyclone associated with the pulse (Figure 3d) are similar to the properties of the cyclone formed during the bolus event in Figures 2a and b.

3.2 Downstream evolution of DSO cyclones

We created composites of the cyclones ($\bar{\zeta} > 0$) along the DSO path to investigate their evolution as they move downstream (Figure 4). The background relative vorticity downstream of Denmark Strait is cyclonic along the entire DSO path (labeled circles in Figure 4a). The anticyclones associated with pulses impact the background relative vorticity, which decreases moving from the Látrabjarg Line to the Denmark Strait South station. Downstream of station #02, where most of the anticyclones spin down, the background relative vorticity monotonically increases moving towards station #07. This is consistent with the hypothesis that PV conservation governs the dynamics in this region (Spall & Price, 1998; von Appen et al., 2014, 2017). Positive relative vorticity is generated in response to the stretching of the water column. Downstream of Denmark

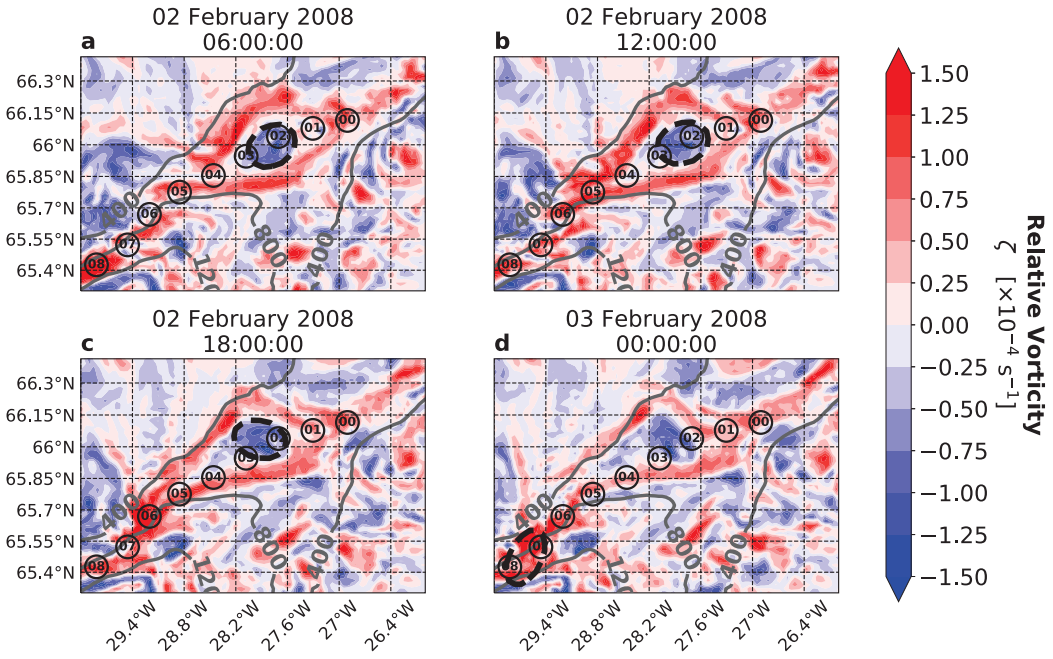

Figure 3. Relative vorticity (ζ) after the pulse event in Figures 2c and d. Four snapshots are shown at 6-hour intervals. Dashed lines bound the vortices detected. Dark gray contours indicate the seafloor depth in meters. Labeled circles indicate the stations along the DSO path. The labeling convention of the DSO stations is the same used in Figure 1. ζ has been extracted along the σ-level at a depth of $5H/8$.

Strait, the light upper layer is constrained at the surface, while the dense DSO is constrained at the bottom. As a result, the mid-level layer is stretched the most, and the relative vorticity peaks near the σ-level along which we extracted the properties of the cyclones. Downstream of station #07, the background relative vorticity decreases as the DSO descends into the Irminger Basin, while the height of the water column continually increases from stations #00 to #17. Therefore, PV conservation is not the dominant mechanism in the region beyond 150 km downstream of the Denmark Strait sill (past station #07). The composites of relative vorticity show the growth and decay phases of the DSO cyclones (black line in Figure 4a). The relative vorticity magnitude of the cyclones is $(0.71\pm0.16)\times10^{-4}$ s^{-1} near the Látrabjarg Line station. As the cyclones move downstream, their relative vorticity grows until they reach station #07, where the relative vorticity is $(1.14\pm0.27)\times10^{-4}$ s^{-1}. Therefore, the growth phase of the DSO cyclones occurs within the first 150 km downstream of Denmark Strait. The decay phase takes place between station #08 and the Spill Jet location #17 (southernmost station). Near the latter, the relative vorticity of the cyclones is $(0.65\pm0.15)\times10^{-4}$ s^{-1}, which is similar to $\bar{\zeta}$ of the cyclones detected near the northernmost station.

The vertical component of the velocity field (w) is shown in Figure 4b. When DSO cyclones are detected (black line), their vertical velocity is of the same magnitude as the background state (labeled circles). However, there is a clear signal in the vertical velocities immediately before and after the detection of the cyclones (blue and red lines, respectively). Six hours before the detection of DSO cyclones, the regions occupied by the vortices are characterized by downwelling ($w < 0$). Conversely, upwelling occurs six hours after the detection. This characteristic behaviour has been reported in studies based on both measurements and numerical models (Magaldi et al., 2011; von Appen et al., 2014). The shape of the upwelling curve (red line in Figure 4b) resembles the relative vorticity curve when cyclones are detected (black line in Figure 4a), and the strongest upwelling occurs near station #8 ($\bar{w} = 0.52 \pm 0.22$ cm s^{-1}). The DSO cyclones growth and decay phases are also evident in the downwelling curve (blue line in Figure 4b). However, between stations #7 and #11, a plateau separates the growth and decay phases, and the maximum downwelling occurs near station #10 ($\bar{w} = -0.54\pm0.27$ cm s^{-1}). The relative vorticity magnitude of the composites extracted six hours before and after the detection of DSO cyclones is higher compared to the background state (Figure 4a), but the curves corresponding to these composites do not show any significant peak. Therefore,

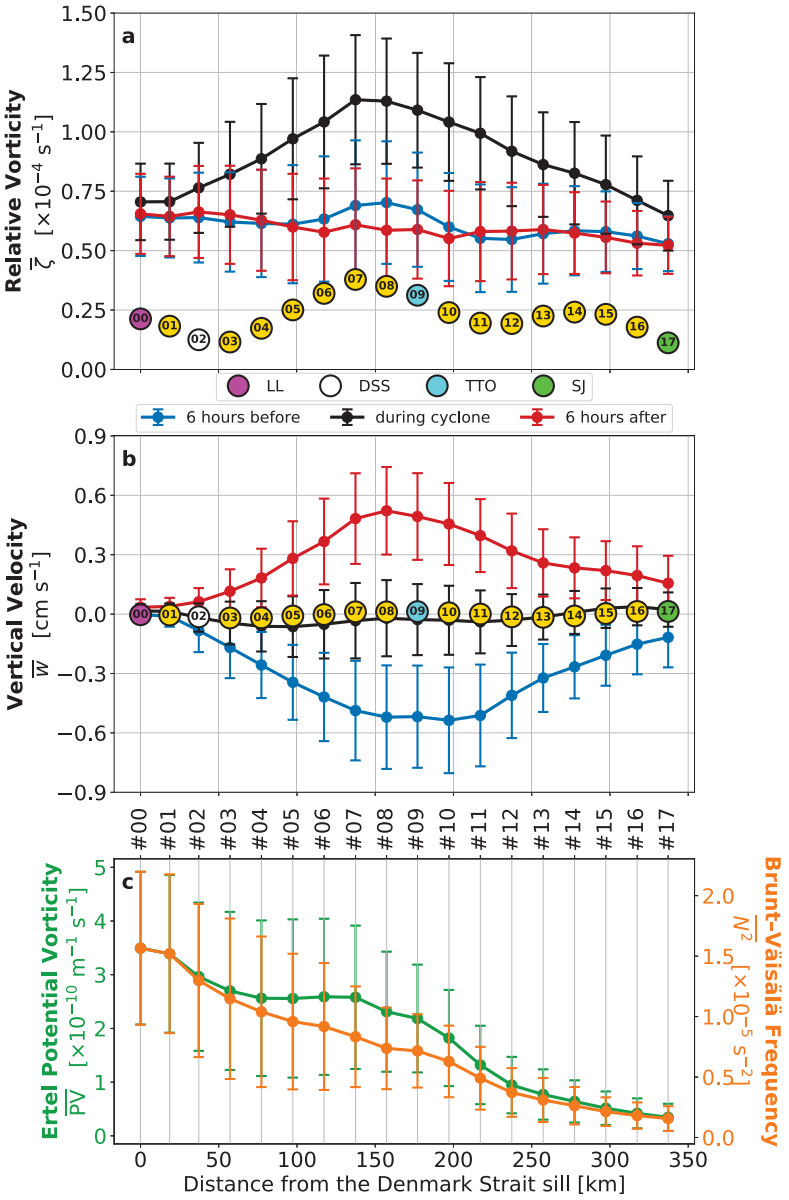

Figure 4. Composites of area-weighted mean (a) relative vorticity, (b) vertical velocity, and (c) Ertel potential vorticity (green, left vertical axis) and Brunt-Väisälä frequency (orange, right axis) along the DSO path. Lines in black (a, b) and green/orange (c) correspond to composites of DSO cyclones. Blue and red lines correspond to composites in the regions of the vortices 6 hours before and after the detection, respectively. Error bars represent the area-weighted standard deviation. Labeled circles correspond to composites of yearly averages in the regions of the vortices (background state). The color code and labeling convention of the DSO stations are the same used in Figure 1. Fields have been extracted along the σ-level at a depth of $5H/8$.

the passage of DSO cyclones is evident in multiple consecutive snapshots, but the highest $\bar{\zeta}$ occurs when $\bar{w}$ changes sign (i.e., transition from downwelling to upwelling). Furthermore, we find that the maximum relative vorticity reached by the DSO cyclones is higher where the rate of change of $\bar{w}$ is higher. The maximum vertical acceleration occurs near station #8 ($\frac{\Delta\bar{w}}{\Delta t} = 2.3 \times 10^{-5}$ m s^{-2}), where the DSO cyclones are mature and manifest the maximum relative vorticity.

The Ertel PV can be approximated as follows (Klinger & Haine, 2019):

$$\mathrm{PV} \approx (f + \zeta)\frac{N^2}{g}, \tag{1}$$

where f is the vertical component of the Coriolis parameter, N is the Brunt-Väisälä frequency, and g is the gravitational acceleration. f does not change significantly within the study region. As a result, the variability of the potential vorticity is controlled by the changes in N^2 and ζ along the DSO path. The Brunt-Väisälä frequency, which is defined by $N^2 = -\frac{g}{\rho_0}\frac{\partial \sigma_\theta}{\partial z}$, decreases as the cyclones move downstream (orange curve in Figure 4c). Therefore, the water in the mid-level layer becomes less stratified as the cyclones descend into the Irminger Basin. The potential vorticity of the DSO cyclones (green curve in Figure 4c) is strongly affected by the decrease of N^2. PV decreases from (3.49±1.42)×10^{-10} m^{-1} s^{-1} near the northernmost station to (0.35±0.25)×10^{-10} m^{-1} s^{-1} near the southernmost station, and N^2 decreases from (1.56±0.63)×10^{-5} s^{-2} to (0.16±0.10)×10^{-5} s^{-2}. However, during the growth stage of the DSO cyclones (between stations #3 and #7), the high relative vorticity of the eddies counterbalances the low stratification due to the stretching of the water column. In particular, the PV only changes by 0.12×10^{-10} m^{-1} s^{-1} in this region. It follows that, downstream of the Denmark Strait South station (#02), the potential vorticity associated with the DSO cyclones is only conserved during the growth phase.

4 Summary and discussion

This study focuses on mesoscale anomalies characteristic of the dense overflow descending from Denmark Strait into the Irminger Basin. We find that boluses are coupled with positive relative vorticity events, whereas pulses are coupled with anticyclonic relative vorticity events. Regardless of their initial sense of rotation, both boluses and pulses trigger the formation of DSO cyclones downstream of Denmark Strait. These find-

245 ings are consistent with the one-to-one relationship between high-transport events and
246 DSO cyclones hypothesized by von Appen et al. (2017).

247 The cyclonic relative vorticity associated with boluses initially increases as these
248 features move downstream. In agreement with Spall and Price (1998) and von Appen
249 et al. (2014), the additional positive relative vorticity gained by these mesoscale features
250 can be explained using conservation of potential vorticity arguments. Specifically, the
251 generation of cyclonic vorticity counterbalances the pronounced stretching of the mid-
252 level layer above the DSO interface, where DSO cyclones are detected. Interestingly, we
253 find that the mechanisms controlling the formation of DSO cyclones associated with pulses
254 are different. The along-stream direction of pulses is oriented toward Greenland com-
255 pared to the orientation of boluses. As the pulses approach shallower regions, their neg-
256 ative relative vorticity is sustained by compression of the water column. The pulses slow
257 down and begin to collapse near the East Greenland shelfbreak. Simultaneously, bands
258 of positive relative vorticity surround the anticyclones. As they weaken, the peripheral
259 bands of positive relative vorticity strengthen and trigger the formation of DSO cyclones
260 to the southwest. Then, the DSO cyclones associated with pulses move southward fol-
261 lowing the DSO path, and gain cyclonic relative vorticity in order to conserve their po-
262 tential vorticity. Regardless of their mechanism of formation, the DSO cyclones detected
263 are found to have similar geometry and strength.

264 The relative vorticity of the cyclones increases over the first 150 km downstream
265 of the sill, then decreases. The eddies are preceded by downwelling and followed by up-
266 welling. The highest vertical velocities coincide with the peak of the cyclones' growth
267 phase, and their highest relative vorticity occurs during the transition from downwelling
268 to upwelling. Furthermore, the rate of change of the vertical velocity associated with the
269 cyclones is proportional to their relative vorticity, suggesting a causal relationship be-
270 tween the vertical acceleration and the strength of the DSO cyclones. The mean strat-
271 ification of the DSO cyclones decreases during their full life cycle, while their initial in-
272 crease in relative vorticity due to stretching is followed by a decrease. As a result, the
273 growth and decay phases of the cyclones are associated with different dynamics, and po-
274 tential vorticity is only materially conserved in the first 150 m downstream of Denmark
275 Strait.

Dense overflows are ubiquitous features in the World Ocean, and our findings could apply to other regions, including the Iceland-Faeroe Passage, the Faeroe Bank Channel, and the Strait of Sicily. An open question is why the potential vorticity associated with DSO cyclones is only conserved during their growth phase. Girton and Sanford (2003) and Voet and Quadfasel (2010) described an increase in DSO entrainment in the region where we find the transition from DSO cyclone growth to decay. In this same region, Koszalka et al. (2017) found the largest warming rate of the overflow. These abrupt changes, combined with the enhanced entrainment and dissipation rates associated with high-transport events (i.e., boluses and pulses; North et al., 2018), might dictate which dynamics dominate the DSO cyclones' evolution at different stages of their life cycle. Further work is needed to understand how these processes affect the variability downstream of our study region, between the Spill Jet section and Cape Farewell.

Acknowledgments

This material is based upon work supported by the National Science Foundation under Grant Numbers OCE-1433448, OCE-1633124, OCE-1756361, and OCE-1756863. The numerical model was run on the Maryland Advanced Research Computing Center (MARCC). Marcello Magaldi helped to configure the model. OceanSpy and several packages from the Pangeo software ecosystem have been used to post-process the model output. The numerical solutions are publicly available on SciServer (`http://sciserver.org`), which is developed and administered by the Institute for Data Intensive Engineering and Science at Johns Hopkins University.

References

Almansi, M., Gelderloos, R., Haine, T. W. N., Saberi, A., & Siddiqui, A. H. (2019). OceanSpy: A Python package to facilitate ocean model data analysis and visualization. *Journal of Open Source Software*, *4*(39), 1506. Retrieved from `http://joss.theoj.org/papers/10.21105/joss.01506` doi: 10.21105/joss.01506

Almansi, M., Haine, T. W. N., Pickart, R. S., Magaldi, M. G., Gelderloos, R., & Mastropole, D. (2017). High-frequency variability in the circulation and hydrography of the denmark strait overflow from a high-resolution numerical model. *Journal of Physical Oceanography*, *47*(12), 2999-3013.

Retrieved from https://doi.org/10.1175/JPO-D-17-0129.1 doi: 10.1175/JPO-D-17-0129.1

Bromwich, D. H., Wilson, A. B., Bai, L., Liu, Z., Barlage, M., Shih, C.-F., ... Walsh, J. E. (2018). The arctic system reanalysis, version 2. *Bulletin of the American Meteorological Society*, *99*(4), 805-828. Retrieved from https://doi.org/10.1175/BAMS-D-16-0215.1 doi: 10.1175/BAMS-D-16-0215.1

Bromwich, D. H., Wilson, A. B., Bai, L.-S., Moore, G. W. K., & Bauer, P. (2016). A comparison of the regional arctic system reanalysis and the global era-interim reanalysis for the arctic. *Quarterly Journal of the Royal Meteorological Society*, *142*(695), 644-658. Retrieved from https://rmets.onlinelibrary.wiley.com/doi/abs/10.1002/qj.2527 doi: 10.1002/qj.2527

Bruce, J. (1995). Eddies southwest of the denmark strait. *Deep Sea Research Part I: Oceanographic Research Papers*, *42*(1), 13 - 29. Retrieved from http://www.sciencedirect.com/science/article/pii/096706379400040Y doi: https://doi.org/10.1016/0967-0637(94)00040-Y

Cooper, L. (1955). Deep water movements in the north atlantic as a link between climatic changes around iceland and biological productivity of the english channel and celtic sea. *Journal of Marine Research*, *14*(4), 347–362.

Dee, D. P., Uppala, S. M., Simmons, A. J., Berrisford, P., Poli, P., Kobayashi, S., ... Vitart, F. (2011). The era-interim reanalysis: configuration and performance of the data assimilation system. *Quarterly Journal of the Royal Meteorological Society*, *137*(656), 553-597. Retrieved from https://rmets.onlinelibrary.wiley.com/doi/abs/10.1002/qj.828 doi: 10.1002/qj.828

Dickson, R. R., & Brown, J. (1994). The production of north atlantic deep water: Sources, rates, and pathways. *Journal of Geophysical Research: Oceans*, *99*(C6), 12319-12341. Retrieved from https://agupubs.onlinelibrary.wiley.com/doi/abs/10.1029/94JC00530 doi: 10.1029/94JC00530

Girton, J. B., & Sanford, T. B. (2003). Descent and modification of the overflow plume in the denmark strait. *Journal of Physical Oceanography*, *33*(7), 1351-1364. Retrieved from https://doi.org/10.1175/1520-0485(2003)033<1351:DAMOTO>2.0.CO;2 doi: 10.1175/1520-0485(2003)033⟨1351:DAMOTO⟩2.0.CO;2

Haine, T. W. N. (2010). High-frequency fluctuations in denmark strait transport. *Geophysical Research Letters*, *37*(14). Retrieved from https://agupubs.onlinelibrary.wiley.com/doi/abs/10.1029/2010GL043272 doi: 10.1029/2010GL043272

Haine, T. W. N., Zhang, S., Moore, G. W. K., & Renfrew, I. A. (2009). On the impact of high-resolution, high-frequency meteorological forcing on denmark strait ocean circulation. *Quarterly Journal of the Royal Meteorological Society*, *135*(645), 2067-2085. Retrieved from https://rmets.onlinelibrary.wiley.com/doi/abs/10.1002/qj.505 doi: 10.1002/qj.505

Harden, B., Pickart, R., Valdimarsson, H., Våge, K., de Steur, L., Richards, C., ... Hattermann, T. (2016). Upstream sources of the denmark strait overflow: Observations from a high-resolution mooring array. *Deep Sea Research Part I: Oceanographic Research Papers*, *112*, 94 - 112. Retrieved from http://www.sciencedirect.com/science/article/pii/S0967063715301266 doi: https://doi.org/10.1016/j.dsr.2016.02.007

Håvik, L., Almansi, M., Våge, K., & Haine, T. W. N. (2019). Atlantic-origin overflow water in the east greenland current. *Journal of Physical Oceanography*, *49*(9), 2255-2269. Retrieved from https://doi.org/10.1175/JPO-D-18-0216.1 doi: 10.1175/JPO-D-18-0216.1

Jochumsen, K., Moritz, M., Nunes, N., Quadfasel, D., Larsen, K. M. H., Hansen, B., ... Jonsson, S. (2017). Revised transport estimates of the denmark strait overflow. *Journal of Geophysical Research: Oceans*, *122*(4), 3434-3450. Retrieved from https://agupubs.onlinelibrary.wiley.com/doi/abs/10.1002/2017JC012803 doi: 10.1002/2017JC012803

Jochumsen, K., Quadfasel, D., Valdimarsson, H., & Jónsson, S. (2012). Variability of the denmark strait overflow: Moored time series from 19962011. *Journal of Geophysical Research: Oceans*, *117*(C12). Retrieved from https://agupubs.onlinelibrary.wiley.com/doi/abs/10.1029/2012JC008244 doi: 10.1029/2012JC008244

Jonsson, S., & Valdimarsson, H. (2004). A new path for the denmark strait overflow water from the iceland sea to denmark strait. *Geophysical Research Letters*, *31*(3). Retrieved from https://agupubs.onlinelibrary.wiley.com/doi/abs/10.1029/2003GL019214 doi: 10.1029/2003GL019214

Jungclaus, J. H., Hauser, J., & Käse, R. H. (2001). Cyclogenesis in the denmark strait overflow plume. *Journal of Physical Oceanography*, *31*(11), 3214-3229. Retrieved from https://doi.org/10.1175/1520-0485(2001)031<3214:CITDSO>2.0.CO;2 doi: 10.1175/1520-0485(2001)031⟨3214:CITDSO⟩2.0.CO;2

Klinger, B. A., & Haine, T. W. N. (2019). *Ocean circulation in three dimensions*. Cambridge University Press. doi: 10.1017/9781139015721

Koszalka, I. M., Haine, T. W., & Magaldi, M. G. (2017). Mesoscale mixing of the denmark strait overflow in the irminger basin. *Ocean Modelling*, *112*, 90 - 98. Retrieved from http://www.sciencedirect.com/science/article/pii/S1463500317300264 doi: https://doi.org/10.1016/j.ocemod.2017.03.001

Krauss, W. (1996). A note on overflow eddies. *Deep Sea Research Part I: Oceanographic Research Papers*, *43*(10), 1661 - 1667. Retrieved from http://www.sciencedirect.com/science/article/pii/S0967063796000738 doi: https://doi.org/10.1016/S0967-0637(96)00073-8

Krauss, W., & Käse, R. H. (1998). Eddy formation in the denmark strait overflow. *Journal of Geophysical Research: Oceans*, *103*(C8), 15525-15538. Retrieved from https://agupubs.onlinelibrary.wiley.com/doi/abs/10.1029/98JC00785 doi: 10.1029/98JC00785

Macrander, A., Käse, R. H., Send, U., Valdimarsson, H., & Jónsson, S. (2007, Apr 01). Spatial and temporal structure of the denmark strait overflow revealed by acoustic observations. *Ocean Dynamics*, *57*(2), 75–89. Retrieved from https://doi.org/10.1007/s10236-007-0101-x doi: 10.1007/s10236-007-0101-x

Magaldi, M. G., Haine, T. W. N., & Pickart, R. S. (2011). On the nature and variability of the east greenland spill jet: A case study in summer 2003. *Journal of Physical Oceanography*, *41*(12), 2307-2327. Retrieved from https://doi.org/10.1175/JPO-D-10-05004.1 doi: 10.1175/JPO-D-10-05004.1

Marshall, J., Adcroft, A., Hill, C., Perelman, L., & Heisey, C. (1997). A finite-volume, incompressible navier stokes model for studies of the ocean on parallel computers. *Journal of Geophysical Research: Oceans*, *102*(C3), 5753-5766. Retrieved from https://agupubs.onlinelibrary.wiley.com/doi/abs/10.1029/96JC02775 doi: 10.1029/96JC02775

Mastropole, D., Pickart, R. S., Valdimarsson, H., Våge, K., Jochumsen, K., &

Girton, J. (2017). On the hydrography of denmark strait. *Journal of Geophysical Research: Oceans*, *122*(1), 306-321. Retrieved from https://agupubs.onlinelibrary.wiley.com/doi/abs/10.1002/2016JC012007 doi: 10.1002/2016JC012007

Medvedev, D., Lemson, G., & Rippin, M. (2016). Sciserver compute: Bringing analysis close to the data. In *Proceedings of the 28th international conference on scientific and statistical database management* (pp. 27:1–27:4). New York, NY, USA: ACM. Retrieved from http://doi.acm.org/10.1145/2949689.2949700 doi: 10.1145/2949689.2949700

Moritz, M., Jochumsen, K., North, R. P., Quadfasel, D., & Valdimarsson, H. (2019). Mesoscale eddies observed at the denmark strait sill. *Journal of Geophysical Research: Oceans*, *0*(ja). Retrieved from https://agupubs.onlinelibrary.wiley.com/doi/abs/10.1029/2019JC015273 doi: 10.1029/2019JC015273

North, R. P., Jochumsen, K., & Moritz, M. (2018). Entrainment and energy transfer variability along the descending path of the denmark strait overflow plume. *Journal of Geophysical Research: Oceans*, *123*(4), 2795-2807. Retrieved from https://agupubs.onlinelibrary.wiley.com/doi/abs/10.1002/2018JC013821 doi: 10.1002/2018JC013821

Okubo, A. (1970). Horizontal dispersion of floatable particles in the vicinity of velocity singularities such as convergences. *Deep Sea Research and Oceanographic Abstracts*, *17*(3), 445 - 454. Retrieved from http://www.sciencedirect.com/science/article/pii/0011747170900598 doi: https://doi.org/10.1016/0011-7471(70)90059-8

Reszka, M. K., Swaters, G. E., & Sutherland, B. R. (2002). Instability of abyssal currents in a continuously stratified ocean with bottom topography. *Journal of Physical Oceanography*, *32*(12), 3528-3550. Retrieved from https://doi.org/10.1175/1520-0485(2002)032<3528:IOACIA>2.0.CO;2 doi: 10.1175/1520-0485(2002)032⟨3528:IOACIA⟩2.0.CO;2

Ross, C. K. (1984). Temperature–salinity characteristics of the overflow water in denmark strait during overflow73. *Rapp. PV Reun. Cons. Int. Explor. Mer*, *185*, 111–119.

Semper, S., Vge, K., Pickart, R. S., Valdimarsson, H., Torres, D. J., & Jnsson, S.

(2019). The emergence of the north icelandic jet and its evolution from north-east iceland to denmark strait. *Journal of Physical Oceanography*, *49*(10), 2499-2521. Retrieved from https://doi.org/10.1175/JPO-D-19-0088.1 doi: 10.1175/JPO-D-19-0088.1

Shi, X. B., Røed, L. P., & Hackett, B. (2001). Variability of the denmark strait overflow: A numerical study. *Journal of Geophysical Research: Oceans*, *106*(C10), 22277-22294. Retrieved from https://agupubs.onlinelibrary.wiley.com/doi/abs/10.1029/2000JC000642 doi: 10.1029/2000JC000642

Spall, M. A., Pickart, R. S., Lin, P., von Appen, W.-J., Mastropole, D., Valdimarsson, H., ... Almansi, M. (2019). Frontogenesis and variability in denmark strait and its influence on overflow water. *Journal of Physical Oceanography*, *49*(7), 1889-1904. Retrieved from https://doi.org/10.1175/JPO-D-19-0053.1 doi: 10.1175/JPO-D-19-0053.1

Spall, M. A., & Price, J. F. (1998). Mesoscale variability in denmark strait: The pv outflow hypothesis. *Journal of Physical Oceanography*, *28*(8), 1598-1623. Retrieved from https://doi.org/10.1175/1520-0485(1998)028<1598:MVIDST>2.0.CO;2 doi: 10.1175/1520-0485(1998)028⟨1598:MVIDST⟩2.0.CO;2

Voet, G., & Quadfasel, D. (2010). Entrainment in the denmark strait overflow plume by meso-scale eddies. *Ocean Science*, *6*(1), 301–310. Retrieved from https://www.ocean-sci.net/6/301/2010/ doi: 10.5194/os-6-301-2010

von Appen, W.-J., Mastropole, D., Pickart, R. S., Valdimarsson, H., Jónsson, S., & Girton, J. B. (2017). On the nature of the mesoscale variability in denmark strait. *Journal of Physical Oceanography*, *47*(3), 567-582. Retrieved from https://doi.org/10.1175/JPO-D-16-0127.1 doi: 10.1175/JPO-D-16-0127.1

von Appen, W.-J., Pickart, R. S., Brink, K. H., & Haine, T. W. (2014). Water column structure and statistics of denmark strait overflow water cyclones. *Deep Sea Research Part I: Oceanographic Research Papers*, *84*, 110 - 126. Retrieved from http://www.sciencedirect.com/science/article/pii/S0967063713002197 doi: https://doi.org/10.1016/j.dsr.2013.10.007

Våge, K., Pickart, R. S., Spall, M. A., Moore, G., Valdimarsson, H., Torres, D. J., ... Nilsen, J. E. Ø. (2013). Revised circulation scheme north of the denmark strait. *Deep Sea Research Part I: Oceanographic Research Papers*, *79*, 20 -

39. Retrieved from http://www.sciencedirect.com/science/article/pii/S0967063713001040 doi: https://doi.org/10.1016/j.dsr.2013.05.007

Weiss, J. (1991). The dynamics of enstrophy transfer in two-dimensional hydrodynamics. *Physica D: Nonlinear Phenomena*, *48*(2), 273 - 294. Retrieved from http://www.sciencedirect.com/science/article/pii/016727899190088Q doi: https://doi.org/10.1016/0167-2789(91)90088-Q

Whitehead, J. A., Stern, M. E., Flierl, G. R., & Klinger, B. A. (1990). Experimental observations of baroclinic eddies on a sloping bottom. *Journal of Geophysical Research: Oceans*, *95*(C6), 9585-9610. Retrieved from https://agupubs.onlinelibrary.wiley.com/doi/abs/10.1029/JC095iC06p09585 doi: 10.1029/JC095iC06p09585

Figure 1.

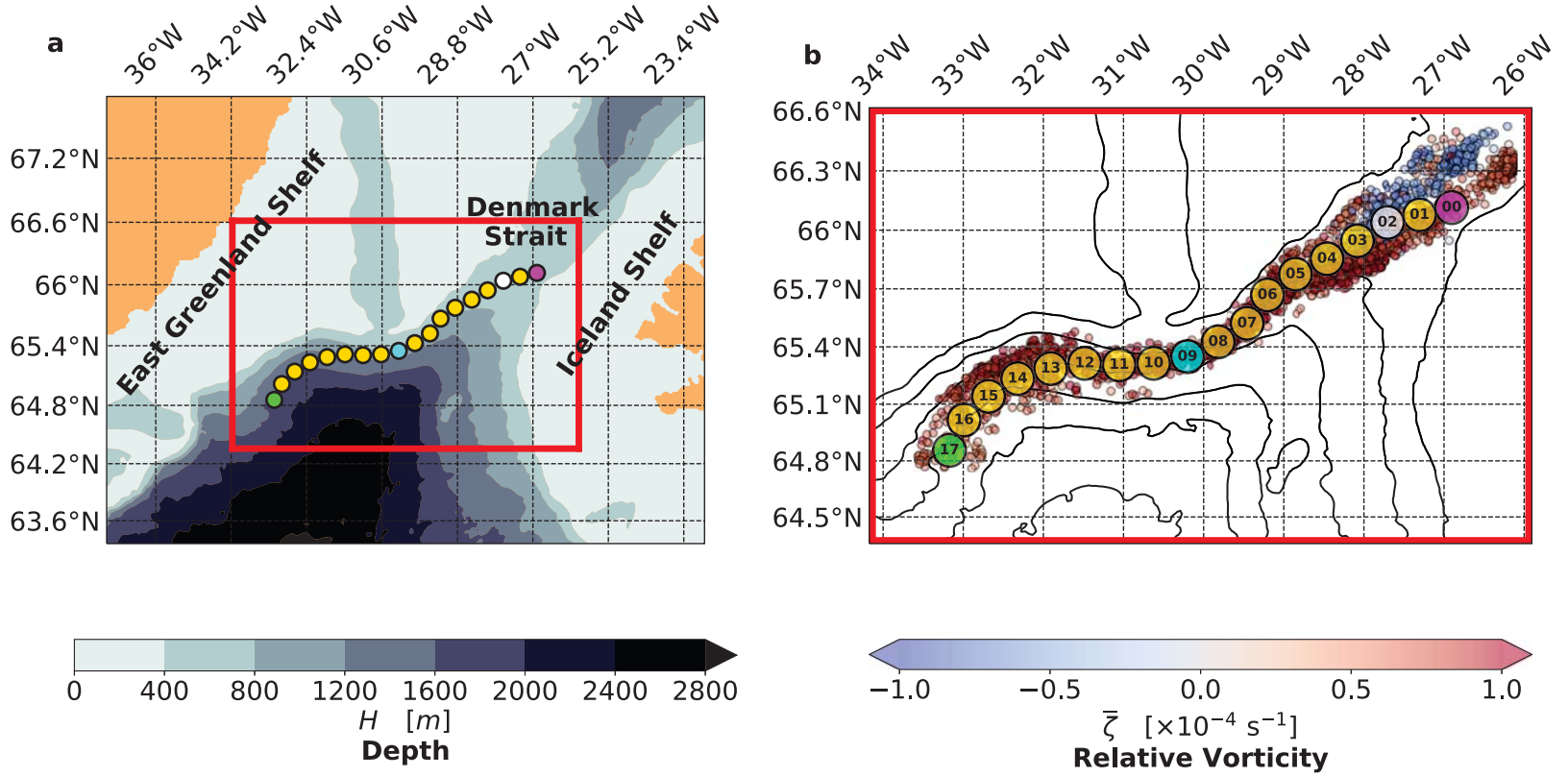
a
36°W
34.2°W
32.4°W
30.6°W
28.8°W
27°W
25.2°W
23.4°W
67.2°N
66.6°N
66°N
65.4°N
64.8°N
64.2°N
63.6°N
East Greenland Shelf
Denmark Strait
Iceland Shelf
0
400
800
1200
1600
2000
2400
2800
H [m]
Depth
b
34°W
33°W
32°W
31°W
30°W
29°W
28°W
27°W
26°W
66.6°N
66.3°N
66°N
65.7°N
65.4°N
65.1°N
64.8°N
64.5°N
00
01
02
03
04
05
06
07
08
09
10
11
12
13
14
15
16
17
−1.0
−0.5
0.0
0.5
1.0
$\overline{\zeta}$ [×10^{-4} s^{-1}]
Relative Vorticity

Figure 2.

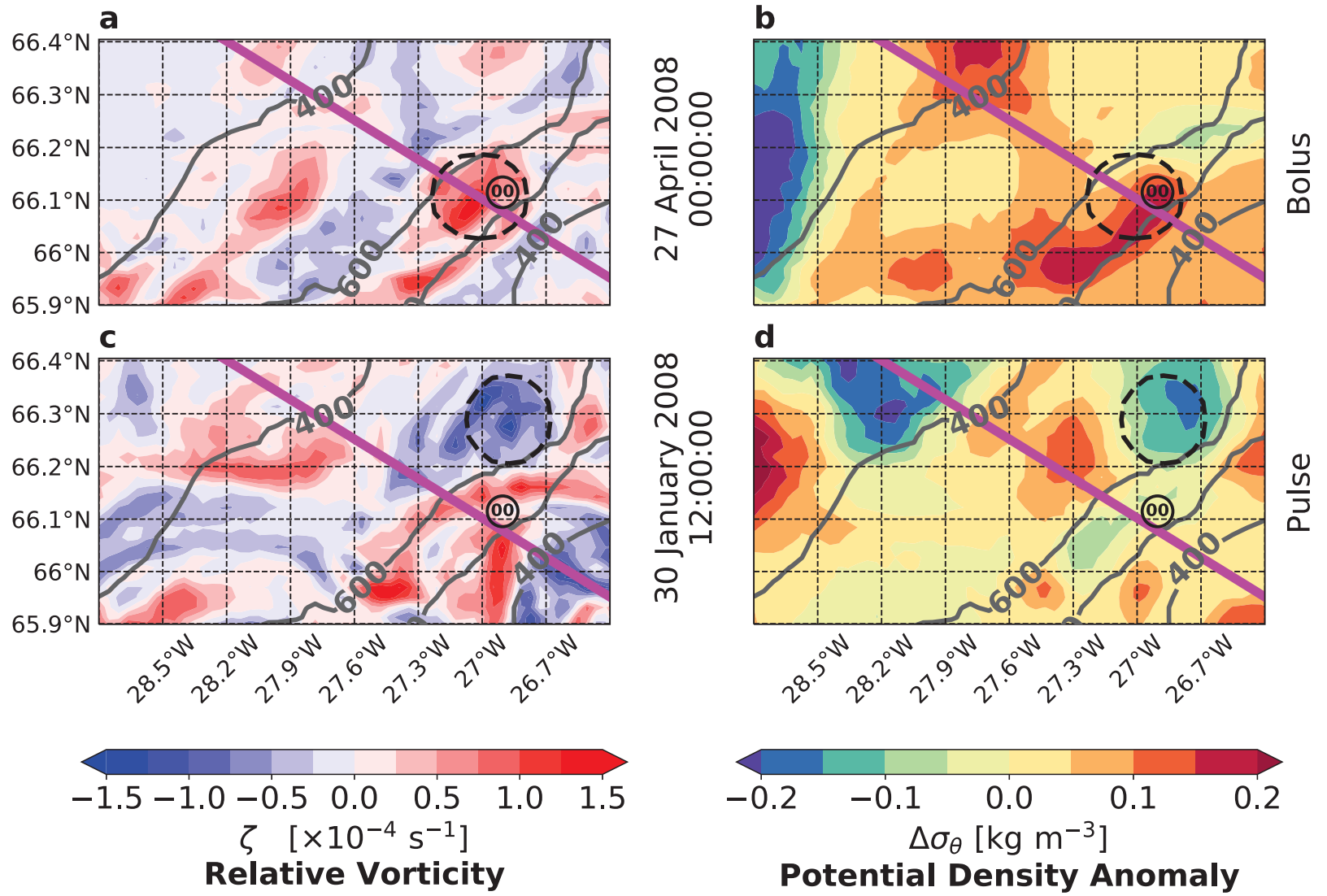
a
b
c
d
66.4°N
66.3°N
66.2°N
66.1°N
66°N
65.9°N
28.5°W
28.2°W
27.9°W
27.6°W
27.3°W
27°W
26.7°W
400
600
00
27 April 2008
00:00:00
30 January 2008
12:00:00
Bolus
Pulse
−1.5 −1.0 −0.5 0.0 0.5 1.0 1.5
ζ [×10⁻⁴ s⁻¹]
Relative Vorticity
−0.2 −0.1 0.0 0.1 0.2
Δσθ [kg m⁻³]
Potential Density Anomaly

Figure 3.

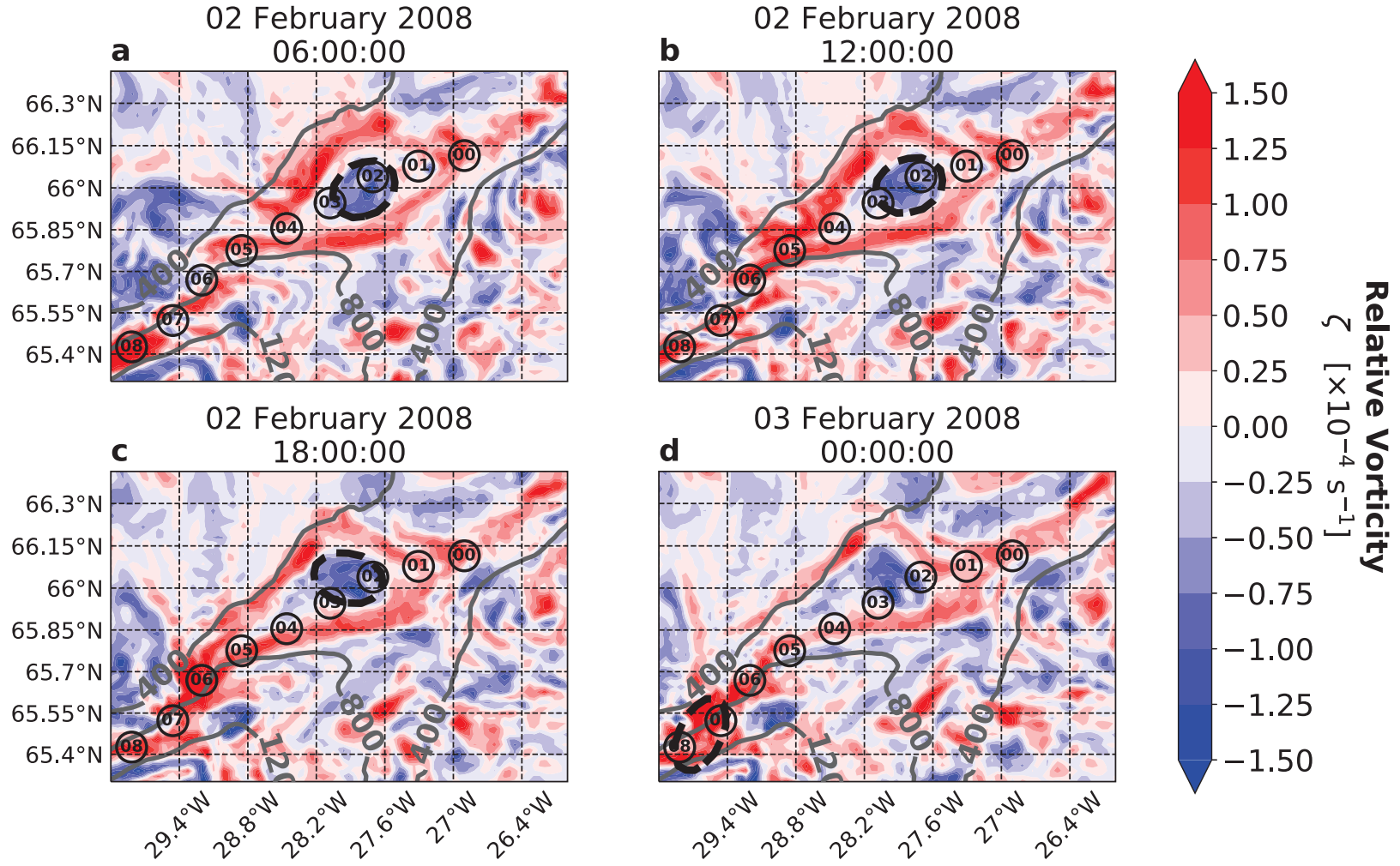
a
02 February 2008
06:00:00
b
02 February 2008
12:00:00
c
02 February 2008
18:00:00
d
03 February 2008
00:00:00
66.3°N
66.15°N
66°N
65.85°N
65.7°N
65.55°N
65.4°N
29.4°W
28.8°W
28.2°W
27.6°W
27°W
26.4°W
400
800
1200
Relative Vorticity
ζ [×10⁻⁴ s⁻¹]
1.50
1.25
1.00
0.75
0.50
0.25
0.00
−0.25
−0.50
−0.75
−1.00
−1.25
−1.50

Figure 4.

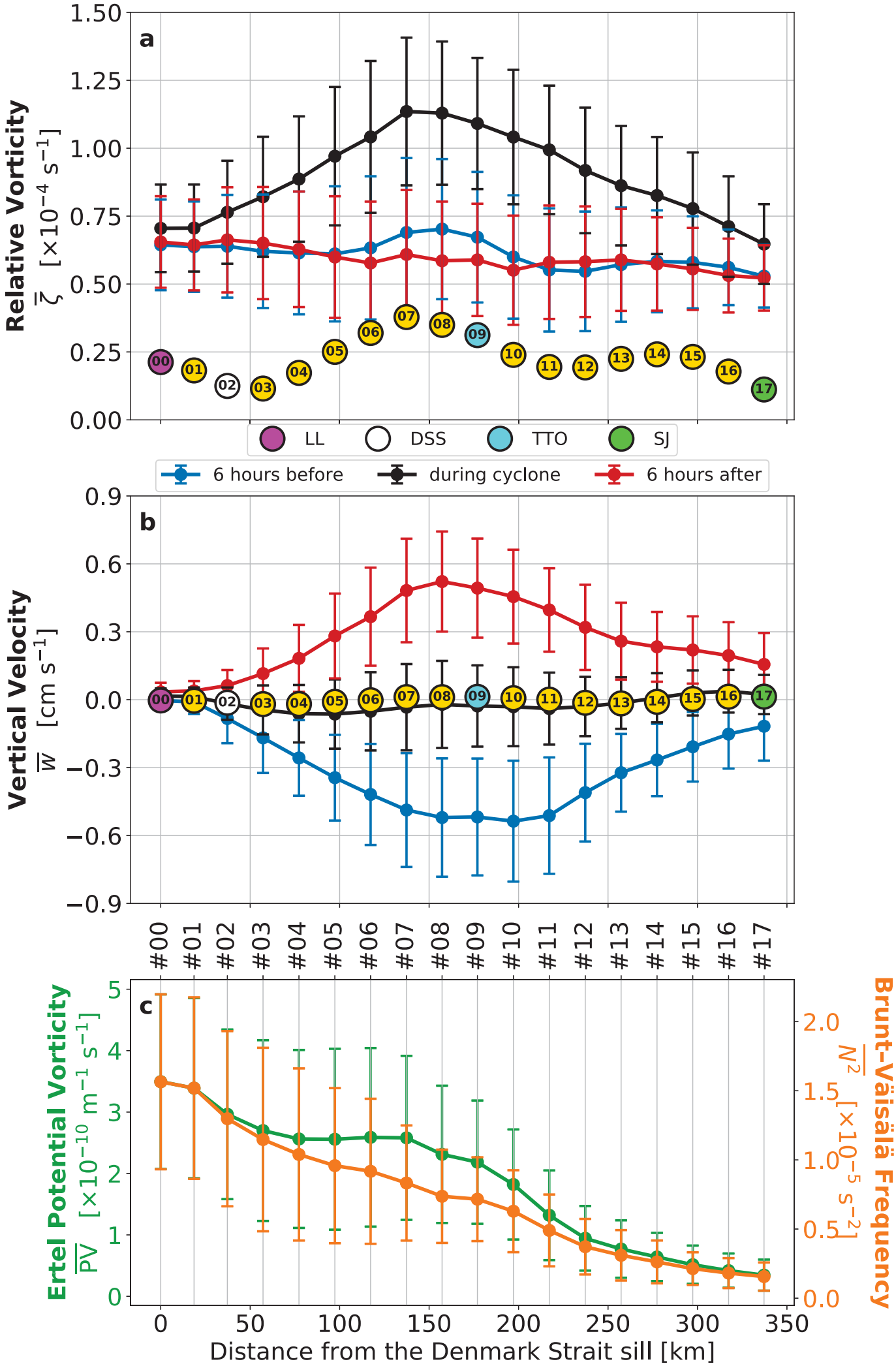
a
Relative Vorticity
$\overline{\zeta}$ [$\times 10^{-4}$ s^{-1}]
1.50
1.25
1.00
0.75
0.50
0.25
0.00
00
01
02
03
04
05
06
07
08
09
10
11
12
13
14
15
16
17
LL
DSS
TTO
SJ
6 hours before
during cyclone
6 hours after
b
Vertical Velocity
$\overline{w}$ [cm s^{-1}]
0.9
0.6
0.3
0.0
−0.3
−0.6
−0.9
#00
#01
#02
#03
#04
#05
#06
#07
#08
#09
#10
#11
#12
#13
#14
#15
#16
#17
c
Ertel Potential Vorticity
$\overline{PV}$ [$\times 10^{-10}$ m^{-1} s^{-1}]
5
4
3
2
1
0
Brunt-Väisälä Frequency
$\overline{N^2}$ [$\times 10^{-5}$ s^{-2}]
2.0
1.5
1.0
0.5
0.0
0
50
100
150
200
250
300
350
Distance from the Denmark Strait sill [km]

Figure SM.

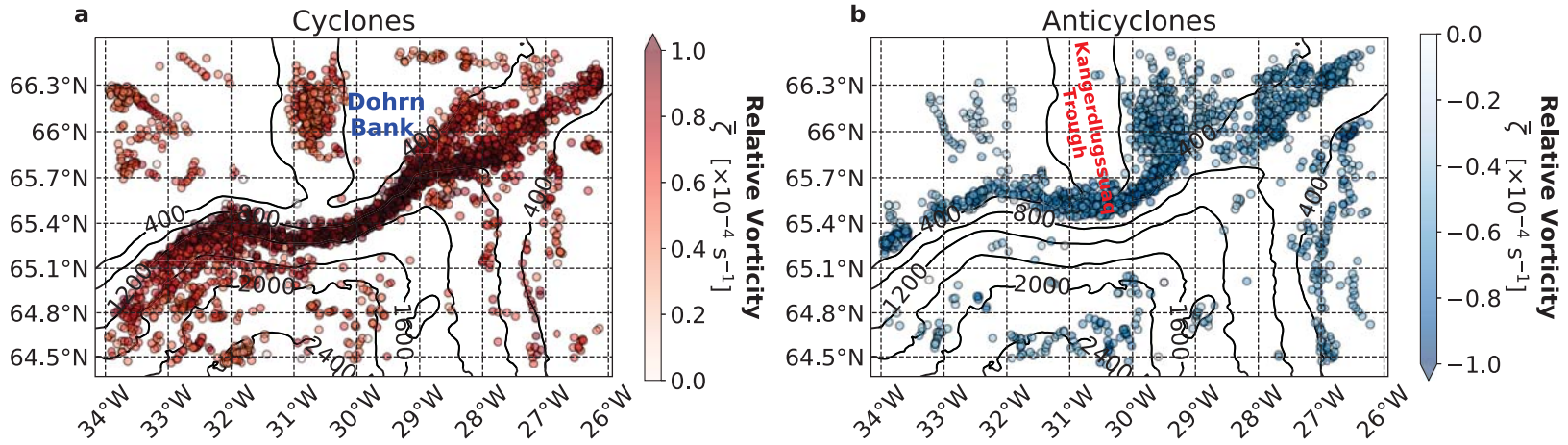
a
Cyclones
Dohrn
Bank
66.3°N
66°N
65.7°N
65.4°N
65.1°N
64.8°N
64.5°N
34°W
33°W
32°W
31°W
30°W
29°W
28°W
27°W
26°W
400
800
1200
2000
1600
2400
1.0
0.8
0.6
0.4
0.2
0.0
Relative Vorticity
ζ [×10⁻⁴ s⁻¹]
b
Anticyclones
Kangerdlugssuaq
Trough
0.0
−0.2
−0.4
−0.6
−0.8
−1.0
Relative Vorticity
ζ [×10⁻⁴ s⁻¹]